Journal of Rock Mechanics and Geotechnical Engineering 11 (2019) 38–45

Contents lists available at ScienceDirect

Journal of Rock Mechanics and Geotechnical Engineering

journal homepage: www.rockgeotech.org

Full Length Article

A comparative study of stress influence on fracture apertures in fragmented rocks

Hossein Agheshlui [a,*], Mohammad H. Sedaghat [b], Siroos Azizmohammadi [c]

[a] Department of Infrastructure Engineering, The University of Melbourne, Victoria, Australia
[b] Centre for Coal Seam Gas, The University of Queensland, Brisbane, Australia
[c] Department of Petroleum Engineering, Montanuniversität Leoben, Leoben, Austria

ARTICLE INFO

Article history:
Received 19 February 2018
Received in revised form
20 April 2018
Accepted 27 May 2018
Available online 17 September 2018

Keywords:
Fracture aperture change
In situ stresses
Frictional interfaces
Ensemble permeability

ABSTRACT

This study compares the calculated fracture apertures in a fragmented rock layer under different stress scenarios using two different approaches. Approach 1 is a simplified method using a two-dimensional (2D) mapping of the fracture network and projects the far-field stresses to individual fractures, and calculates the dilation, normal and shear displacements using experimental stiffnesses available in the literature. Approach 2 employs a three-dimensional (3D) finite element method (FEM) for the mechanical analysis of the fragmented rock layer considering the interaction with the neighbouring rock layers, frictional interfaces between the rock blocks, stress variations within the fragmented rock layer, and displacements, rotations and deformations of rock blocks. After calculating the fracture apertures using either of the approaches, the permeability of the fragmented rock layer is calculated by running flow simulations using the updated fracture apertures. The comparison between the results demonstrates an example of the inaccuracies that may exist in methods that use simplified assumptions such as 2D modelling, ignoring the block rotations and displacements, projected far-field stresses on fractures, and the stress variations within the rock layer. It is found that for the cases considered here, the permeability results based on apertures obtained from the simplified approach could be 40 times different from the results from apertures calculated using a full mechanical approach. Hence, 3D mechanical modelling implementing realistic boundary conditions, while considering the displacements and rotations of rock blocks, is suggested for the calculation of apertures in fragmented rocks.

1. Introduction

Previous studies suggest that the hydraulic conductivity of a fracture network in moderate compressive stress levels can significantly vary due to the change of fracture apertures caused by the applied stresses (Barton et al., 1985; Zhang and Sanderson, 1996; Zhang et al., 2002; Lang et al., 2012; Latham et al., 2013). Ensemble permeability can increase or decrease depending on the orientation and magnitude of horizontal stresses and the level of fluid pressure (Min et al., 2004). This change is of critical importance in several engineering fields, especially in petroleum engineering as it can affect the production of hydrocarbons. Hydraulic conductivity of fractured rocks is a function of fracture apertures, surface roughness and contact area, all of which can change due to the applied stresses. From these factors, the change of aperture was the focus of this study.

Estimation of fracture change due to the applied stresses is a complex problem. There are several models developed using different simplified assumptions. For example, some models ignore block deformations, displacements and rotations, while some two-dimensional (2D) models ignore the influence of stresses in the normal direction when modelling the fracture network, and others do not consider the stress variations within a rock layer when resolving the far-field stresses on fractures.

Zhang and Sanderson (1996) studied the effect of stress on the permeability of a fracture network by applying different levels of differential stresses and loading directions in an implementation, i.e. the universal distinct element code (UDEC). Their model can consider the deformation of the blocks and their displacement and

* Corresponding author.
E-mail addresses: Hossein.agheshlui@unimelb.edu.au (H. Agheshlui), m.sedaghat@uq.edu.au (M.H. Sedaghat), siroos.azizmohammadi@unileoben.ac.at (S. Azizmohammadi).

Peer review under responsibility of Institute of Rock and Soil Mechanics, Chinese Academy of Sciences.

https://doi.org/10.1016/j.jrmge.2018.05.003

rotation. The interaction between the blocks is defined using normal and shear stiffnesses. Results obtained from their research showed the importance of the magnitude of the horizontal stresses dependent on burial depth, the difference between the minimum and maximum horizontal stresses, and the orientation of the horizontal stresses. However, their study did not consider the stress variations within the fractured rock layer due to the interaction between the blocks where stress concentrations are created. As the modelling was implemented in 2D, the actual triaxial stress states were not considered subsequently. Also, the influence of the mechanical behaviour of the neighbouring layers was ignored inevitably.

Dual continua methods are also commonly used in the coupling simulation of flow and mechanics for flow in fractured rocks. Zhang et al. (2002), in a 2D simulation, defined the fracture and matrix as a large number of small blocks connected at their boundaries with tensile and shear stress limits defined at boundaries. The broken connections acted as flow path. They showed that higher differential stresses and fracture pressures can initiate fractures and grow the existing fractures. Similarly, this study did not consider the triaxial stress states and the influence of the neighbouring rock layers.

Lei et al. (2017) conducted a three-dimensional (3D) study on the influence of stress on permeability of the fractured rocks. They used a discrete element method (DEM) which considered the block deformations, stress fields in the fractured rock layer and fracture propagation. The influence of neighbouring layers was not considered in this study.

Azizmohammadi and Matthai (2017) applied the classical Barton and Bandis model (1982) to compute in situ fracture aperture patterns for naturally fractured rock samples mapped in outcrops (m to km scale) where the aperture varied along fractures. They calculated the fracture apertures using the far-field stresses projected on fracture planes. Their study was also performed in 2D and did not consider the stress variations within the rock layer.

Agheshlui and Matthai (2017) developed a 3D mechanical model which included a fragmented rock layer sandwiched between two plastic shale layers. The mechanical model considered the interaction between the three rock layers, frictional interfaces between the rock blocks, and the stress variations within the fragmented rock layer. Using this 3D model incorporating neighbouring layers, realistic boundary conditions were applied to the fragmented rock layer. Also, block deformations, displacements and rotations were considered conducting the stress–strain analysis of the entire model having frictional interfaces defined between rock blocks as well as rock layers.

In this study, results from two different approaches (i.e. Agheshlui and Matthai, 2017; Azizmohammadi and Matthai, 2017) are compared to quantify the magnitude of errors that may occur if simplified assumptions such as those mentioned above are used. A fragmented rock layer is analysed by the method developed by Azizmohammadi and Matthai (2017) and the model developed by Agheshlui et al. (2018). Two different depths and two levels of differential horizontal stresses are considered. The fracture maps for these cases are obtained and then used to obtain permeability matrices.

2. Methodology

The method used for both approaches discussed here for calculation of ensemble permeability includes two steps. In the first step, the apertures of the fragmented rock layer are calculated applying different in situ stress scenarios. Then a single-phase flow analysis is performed to obtain the permeability tensor for the fragmented rock layer with the calculated apertures. The calculation of fracture apertures using the two different approaches is briefly discussed below. A more detailed discussion on the two approaches can be found in Azizmohammadi and Matthai (2017) and Agheshlui and Matthai (2017).

2.1. Fracture aperture calculation using approach 1

Approach 1 calculates fracture apertures for 2D models by projecting the in situ horizontal stresses on the fracture walls. This approach ignores the overburden stress and the stress variations within the rock layer as well as the deformations, displacements, and rotations of rock blocks. For the calculation of the aperture changes under the far-field stresses, this method uses Barton et al. (1985) fracture roughness as described below:

$$a = a_0 - \delta_n + \delta_d \tag{1}$$

where a_0 is a closure aperture under stress-free conditions, δ_n is the reduction of aperture caused by the normal stress applied to it, and δ_d is the increase of aperture due to shear dilation. A small value is assigned for a_0 to ensure that all fractures in the pattern have initial non-zero apertures.

Normal closure, δ_n, can be calculated by Bandis' hyperbolic model (Bandis et al., 1983):

$$\delta_n = \frac{k_{n0} c_m^2}{k_{n0} c_m + \sigma_{eff}} \tag{2}$$

where σ_{eff} is the effective normal stress acting on the fracture plane, c_m is the maximum closure, and k_{n0} is the initial fracture normal stiffness. These parameters can be estimated using the empirical relations introduced by Bandis et al. (1983).

The mobilisation of the joint roughness results in fracture dilation which is experimentally expected to occur at 30% of the peak shear displacement (Barton et al., 1985). Hence, the shear dilation, δ_d, can be correlated with the shear displacement, σ_s, and the mobilised dilation angle, $\phi_{d,mob}$, by

$$\delta_d = \delta_s \tan\phi_{d,mob} \tag{3}$$

The mobilised dilation angle $\phi_{d,mob}$ is evaluated by

$$\phi_{d,mob} = \frac{1}{M} JRC_{mob} \log_{10}\left(\frac{JCS_n}{\sigma_{eff}}\right) \tag{4}$$

where JCS_n is the joint compressive strength.

The coefficient M characterises the damage and can be obtained from Barton and Choubey (1977):

$$M = 0.7 + JRC_n \Big/ \left[12 \log_{10}\left(\frac{JCS_n}{\sigma_{eff}}\right)\right] \tag{5}$$

The parameter JRC_{mob} is the mobilised joint roughness coefficient which can be estimated by

$$JRC_{mob} = \left[\tan^{-1}\left(\frac{\sigma_s}{\sigma_{eff}}\right) - \phi_r\right] \Big/ \log_{10}\left(\frac{JCS_n}{\sigma_{eff}}\right) \tag{6}$$

where ϕ_r is the residual friction angle.

The fracture length dependent characteristics, joint roughness coefficient, JRC_n, and joint compressive strength, JCS_n were introduced by Barton and Bandis (1982) to address the influence of fracture size on surface properties. Since the required rock joint parameters for the computation of fracture aperture using Approach 1 are not available for the described fractured rock, plausible constant values were assumed in this context: joint

roughness coefficient, $JRC_0 = 10$; joint wall compressive strength, $JCS_0 = 75$ MPa; and a residual friction angle, $\phi_r = 25°$.

2.2. Fracture aperture calculation using approach 2

In Approach 2, a full 3D finite element mechanical modelling of the fragmented rock layer and its neighbouring layers located above and below the fragmented layer was conducted. The fragmented rock layer was modelled using individual blocks defined separately and placed next to each other with their interactions modelled using frictional interfaces. Frictional interfaces were also defined between the rock layers to create realistic boundary conditions in order to consider the influence of the difference between the mechanical properties of the rock layers. Due to the deformation, displacement and rotation of the blocks under the applied stresses, openings could develop between the blocks. This comprises the first component of the fracture aperture. The second component is the fracture dilation which is calculated as explained in Section 2.2.2. With these two components added, the fracture aperture is calculated in Approach 2.

The finite element modelling was conducted using ABAQUS™. To solve the linear elasticity equations, a displacement based elastic finite element method (FEM) was used. Static equilibrium was described by Cauchy's equation in vectorial form (Malvern, 1969):

$$\nabla \underline{\boldsymbol{\sigma}} + \boldsymbol{f} = \boldsymbol{0} \tag{7}$$

where $\underline{\boldsymbol{\sigma}}$ is the 3×3 order stress tensor and $\boldsymbol{f}$ is the applied vector of body forces. In general $\sigma_{ij} = \sigma_{ji}$, hence only six of the components of the stress tensor are unknown. However, the equilibrium equations provide only three equations. The other three equations can be obtained from Hooke's law relating displacements to strains and in turn to stresses:

$$\underline{\boldsymbol{\sigma}} = \underline{\boldsymbol{C}}\underline{\boldsymbol{\varepsilon}} \tag{8}$$

where $\underline{\boldsymbol{\varepsilon}}$ is the strain tensor and, in the most general case, $\underline{\boldsymbol{C}}$ is a fourth-order six-by-six tensor. By substituting Eq. (8) into Eq. (7), the latter can be solved. Then Eq. (7) can be written as

$$\nabla \underline{\boldsymbol{C}} \nabla \underline{\boldsymbol{\varepsilon}} + \boldsymbol{f} = 0 \tag{9}$$

Here, the influence of the pore pressure within the fragmented rock layer was not considered on the deformation of the blocks. This was done to decrease the computational cost. It also does not influence the deviatoric deformation of the rock blocks as the fluid pressure only affects the normal components of the stress tensor.

2.2.1. Frictional interfaces

Frictional interfaces were defined between the rock layers and at the interfaces between the rock blocks. A penalty algorithm was used in the normal direction to avoid penetration and a frictional behaviour was defined in the tangential direction. A basic Coulomb friction model was used with the tangential stress required for sliding given by the following equation (Coulomb, 1773):

$$\tau = \mu_f \left(\sigma_n - p_p \right) \tag{10}$$

where τ is the tangential stress, σ_n is the normal stress, p_p is the fluid pressure, and μ_f is the friction coefficient. For a very wide range of rock types at relatively high effective normal stresses ($\sigma_{eff} \geq \sim 10$ MPa), friction on faults is independent of surface roughness, normal stress, slip rate, etc., and is generally between 0.6 and 1 (Byerlee, 1978). Here, a value of 0.6 is used conservatively. Note that the fracture pressure reduces the effective normal stress applied to an interface, consequently the tangential stress can be sustained by an interface. For an earlier implantation of frictional interfaces between rock layers, please see Agheshlui and Matthai (2017).

2.2.2. Dilation effect

Models developed based on the experimental data available in the literature (Bandis et al., 1983) are used for the estimation of the dilation effect on the fracture apertures in Approach 2. The Bandis model provides the dilation values based on the shear displacement under different levels of normal stresses applied to the fracture walls. The joint roughness coefficient $JRC_0 = 10$, joint wall compressive strength $JCS_0 = 75$ MPa and unconfined rock compressive strength $UCS = 150$ MPa were used.

2.3. Comparison of two approaches used for fracture aperture calculation

Table 1 highlights the important differences between the two approaches used in this study.

To calculate the ensemble permeability, fracture aperture maps were obtained using both approaches in a 2D model to conduct single-phase flow analyses in two perpendicular directions. The analysis was conducted in 2D to limit the difference between the two approaches in order to calculate the fracture apertures. Furthermore, the flow in the direction perpendicular to the fragmented rock layer was expected to be minimal. This analysis was conducted using complex systems modelling platform (CSMP++) (Matthai et al., 2012, 2014). A discrete fracture and matrix (DFM) model was used for flow analysis. For this, the fractures were represented by lower dimensional elements compared to the matrix (Paluszny et al., 2007; Matthai and Nick, 2009). Having computed the aperture of the fractures, a, the permeability of individual fractures, k_f, was determined using the parallel plate law (Kranzz et al., 1979):

$$k_f = \frac{a^2}{12} \tag{11}$$

Two flow problems were solved in two perpendicular directions in order to obtain the full ensemble permeability tensor, $\boldsymbol{k}^E$, given by Eq. (12). This required solving Darcy's law, Eq. (13), modified for the volume-averaged fluid velocity ($\boldsymbol{u}$), pressure gradient (∇p), and viscosity (μ):

Table 1
Comparison of the approaches used for calculation of fracture apertures.

Approach	Modelling dimensions	Overburden stress	Influence of neighbouring layers	Stress variations in the fragmented rock layer	Block rotations, displacements, and deformations
1	2D	Not considered	Not considered	Not considered. Far-field stresses are directly projected to fracture walls	Not considered
2	3D	Considered	Considered	Considered	Considered

$$\boldsymbol{k}^E = \begin{bmatrix} k^E_{xx} & k^E_{xy} \\ k^E_{yx} & k^E_{yy} \end{bmatrix} \tag{12}$$

$$\langle \boldsymbol{u} \rangle = -\frac{\boldsymbol{k}^E}{\langle \mu \rangle} \langle \nabla p \rangle \tag{13}$$

where $\langle\ \rangle$ is the volume averaging operator (Durlofsky, 1992).

Eq. (13) in matrix form can be written as

$$\begin{bmatrix} \langle \nabla p_x \rangle^1 & \langle \nabla p_y \rangle^1 & 0 & 0 \\ 0 & 0 & \langle \nabla p_x \rangle^1 & \langle \nabla p_y \rangle^1 \\ \langle \nabla p_x \rangle^2 & \langle \nabla p_y \rangle^2 & 0 & 0 \\ 0 & 0 & \langle \nabla p_x \rangle^2 & \langle \nabla p_y \rangle^2 \end{bmatrix} \begin{Bmatrix} k^E_{xx} \\ k^E_{xy} \\ k^E_{yx} \\ k^E_{yy} \end{Bmatrix} = -\langle \mu \rangle \begin{Bmatrix} \langle u_x \rangle^1 \\ \langle u_y \rangle^1 \\ \langle u_x \rangle^2 \\ \langle u_y \rangle^2 \end{Bmatrix} \tag{14}$$

where superscripts 1 and 2, respectively, denote the two flow problems solved in two perpendicular directions as explained earlier.

3. Model description

The model used here consisted of a 2D 4.5 m × 4 m section of Kilve outcrop as shown in Fig. 1. This 2D fragmented brittle limestone rock was directly used for the analyses conducted in Approach 1. For analyses performed using Approach 2, the 2D fragmented rock layer was extruded to a thickness of 0.2 m to build a 3D model. To consider the influence of the neighbouring layers and to apply realistic boundary conditions, the 3D fragmented rock layer was sandwiched between two plastic layers. The in situ stresses for the 3D model were applied to the side walls of the model as depicted in Fig. 1. Horizontal stresses were applied with an angle of 45° from the horizontal axis to create dilation effect in the model.

The hydro-mechanical properties of the rock layers of the model are given in Table 2.

Table 2
Hydro-mechanical properties of rock layers used in the model.

Rock type	Elastic modulus (GPa)	Poisson's ratio	Porosity	Permeability (m^2)
Shale	10	0.4	0.05	1×10^{-14}
Limestone	20	0.25	0.15	1×10^{-13}

3.1. Loading scenarios

Four different loading scenarios were considered for the comparison of the fracture aperture map and the ensemble permeability of the model using the two different approaches. These included two different burial depths and two different horizontal stress conditions. The average dry rock density above the fragmented rock layer was assumed to be 2200 kg/m^3 and the fluid pressure was assumed to be hydrostatic with a brine density of 1200 kg/m^3. Table 3 lists all the considered cases.

To demonstrate the level of inaccuracies that may occur when using Approach 1, large differences between the maximum and minimum horizontal stresses were selected. Studies show that the difference between horizontal stresses can have a significant influence on the fracture apertures (Zhang and Sanderson, 1996). In an area of critically stressed normal faults, when the pore pressure is hydrostatic, the lower bound value of the minimum principal stress $\sigma_h \approx 0.6\sigma_v$ (Zoback, 2007), which is thus selected as the minimum horizontal stress.

3.2. Flow modelling

Finite element centred finite volume (FECFV) simulator developed on the basis of CSMP++ (Bazrafkan and Matthai, 2011) was

Table 3
Physico-mechanical and hydraulic properties of rock layers used in the model.

Case	Burial depth (m)	Overburden stress, σ_v (MPa)	Maximum horizontal stress, σ_H (MPa)	Minimum horizontal stress, σ_h (MPa)	Fluid pressure (MPa)
1	500	10.79	$0.9\sigma_v = 9.71$	$0.6\sigma_v = 6.47$	5.88
2	500	10.79	$0.9\sigma_v = 9.71$	$0.65\sigma_v = 7.01$	5.88
3	1500	32.36	$0.9\sigma_v = 29.13$	$0.6\sigma_v = 19.42$	17.65
4	1500	32.36	$0.9\sigma_v = 29.13$	$0.65\sigma_v = 21.04$	17.65

Note: Load scenarios consistent with 500 m depth were used and 4 different cases were considered adequate to demonstrate the point on the inaccuracy of the simplified methods.

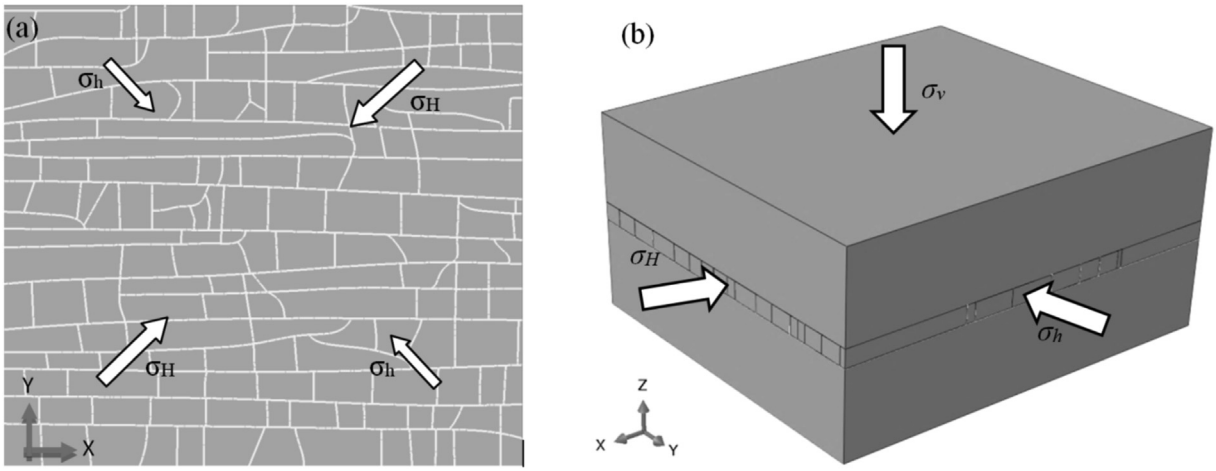

Fig. 1. Extruded fragmented rock layer sandwiched between two soft shale layers in 3D.

Table 4
Boundary conditions for each single-phase flow scenario.

Case	Flow problem	p^{left} (Pa)	p^{right} (Pa)	p^{bottom} (Pa)	p^{top} (Pa)
1	1st	20,000	19,010	–	–
	2nd	–	–	20,000	19,120
2	1st	20,000	19,010	–	–
	2nd	–	–	20,000	19,120
3	1st	20,000	19,010	–	–
	2nd	–	–	20,000	19,120
4	1st	20,000	19,010	–	–
	2nd	–	–	20,000	19,120

used to model fluid flow on a DFM model (Fig. 1a). All the fractures were assumed to be fully developed over the thickness of the limestone layer. The rock properties and saturation were discretised as piecewise constants on the elements while fluid pressure was discretised as piecewise linear on the nodes and computed with the FEM (e.g. Zienkiewicz, 1977).

In Approach 2 for each loading scenario, a geomechanical modelling was conducted to calculate the fracture apertures on all the sidewalls of all the blocks. These apertures were then input into the flow simulations. Fractures with apertures smaller than 0.025 mm were assumed to be closed and their properties were assumed to be equal to that of the matrix (matrix permeability $k_m = 10^{-13}$ m^2, and matrix porosity $\phi_m = 0.2$).

For each flow problem, constant pressure Dirichlet boundary conditions were applied to the model boundaries perpendicular to that direction, and a pressure gradient of 220 Pa/m was applied while no-flow (natural) boundary conditions were defined at the other two edges (Table 4) (see Sedaghat et al., 2017). Having the solved pressure field, the velocity field was calculated by post-

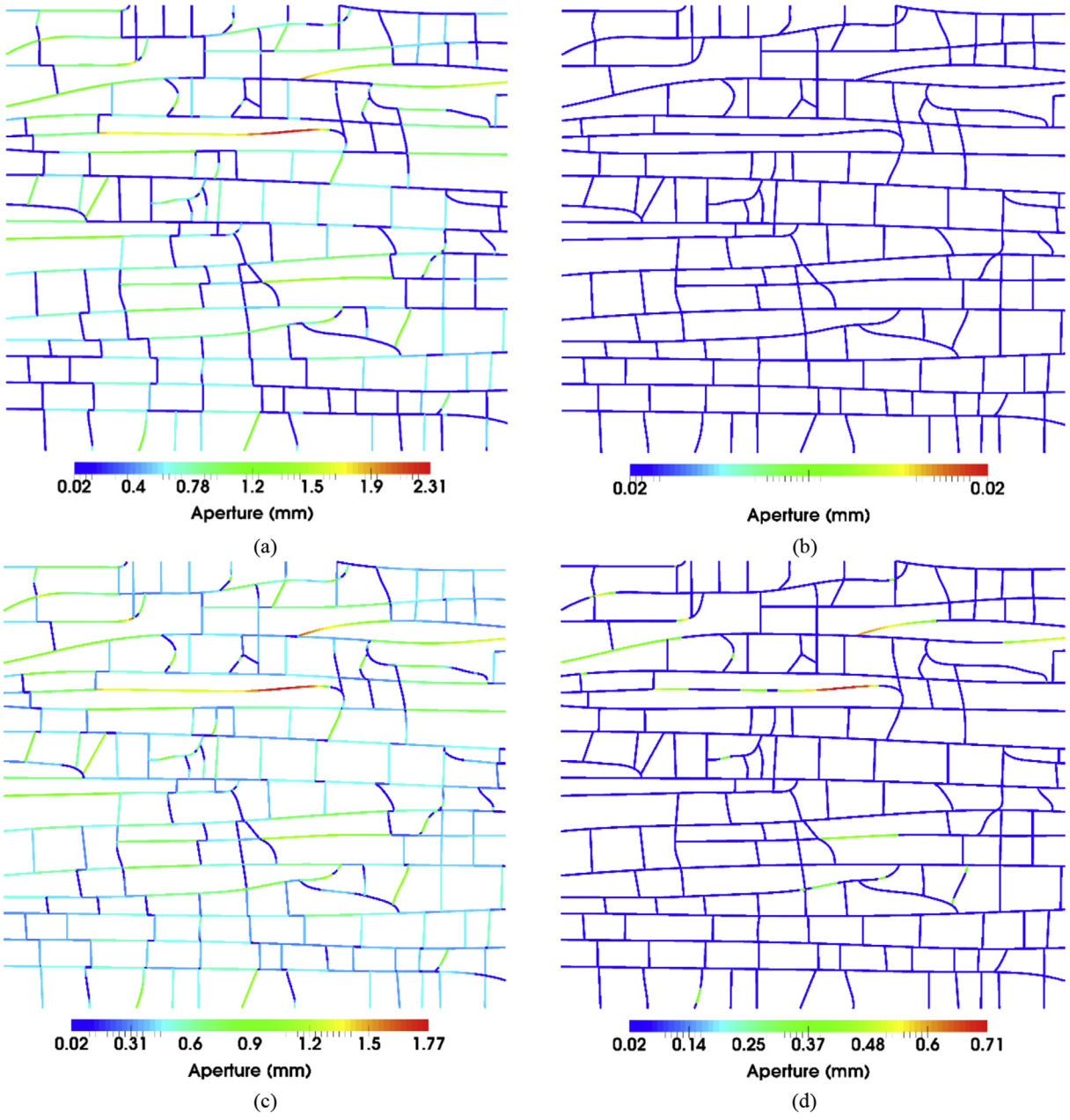

Fig. 2. Fracture aperture maps obtained using Approach 1: (a) case 1; (b) case 2 (for case 2, all fractures are closed); (c) case 3; and (d) case 4.

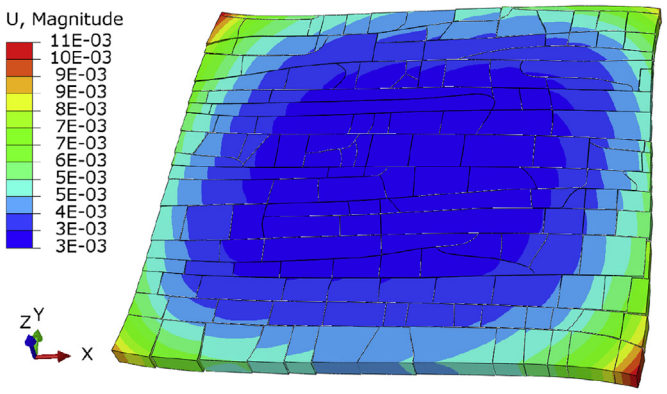

Fig. 3. Deformation shapes of the fragmented rock layer under overburden and horizontal stresses - Case 1. *U* is the displacement (m) and deformations are 20 times magnified.

processing the pressure gradients using Darcy's law. The brine viscosity used in this study was assumed to be 0.001 Pa s.

4. Results

Fig. 2 presents the aperture maps obtained for the model using Approach 1. It can be seen that for both depths, as σ_h increases from $0.6\sigma_v$ to $0.65\sigma_v$ (case 1 vs. case 2 and case 3 vs. case 4), most of the fractures become closed. Comparing case 1 vs. case 3, and case 2 vs. case 4, fewer fractures tend to be open in the shallower depth.

Fracture aperture maps using Approach 2 were obtained by the stress–strain analysis of the model as shown in Fig. 1b. The deformed shape of the model for case 1 is depicted in Fig. 3. The normal and shear displacements were calculated based on the gap created and the relative shear displacements between the blocks. The dilation was calculated based on the normal stress applied to the fracture walls and the shear displacement occurred at fracture segments using Bandis et al. (1983)'s model. The fracture aperture maps obtained from Approach 1 are shown in Fig. 4.

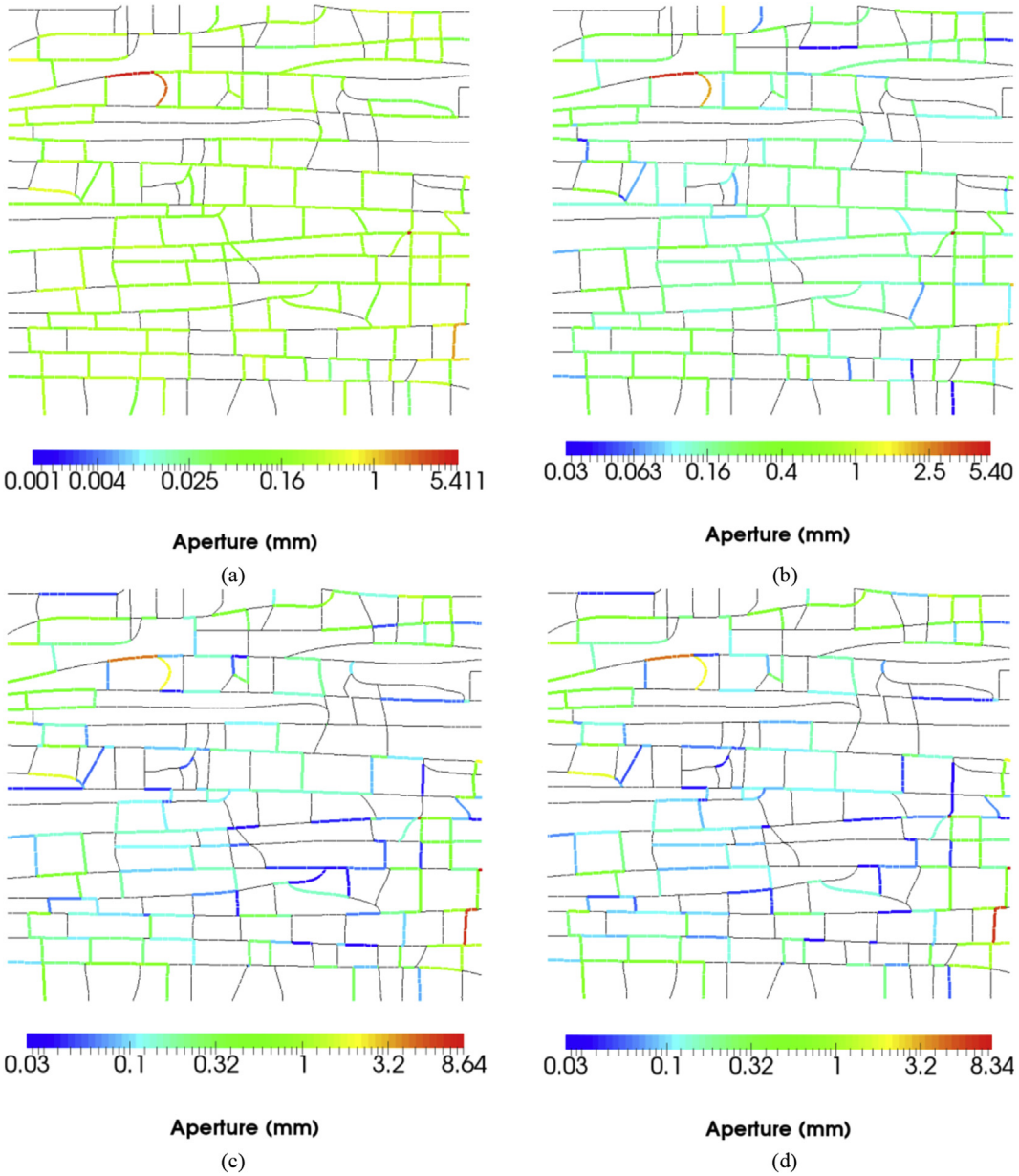

Fig. 4. Fracture aperture maps obtained using Approach 2: (a) case 1, (b) case 2, (c) case 3, and (d) case 4.

In comparison to the results from Approach 1 (see Fig. 2), Approach 2 has resulted in more open fractures with larger maximum apertures for all cases, except for case 3 from Approach 1 which has an unexpected highly developed network. In the results of Approach 2, open fractures have created a network even for the cases with $\sigma_h = 0.65\sigma_v$ in which their fractures were almost closed in Approach 1. Unlike the results obtained from Approach 1, the number of open fractures decreases with depth. Also, the results are not as sensitive as the ones from Approach 1 to small changes in the minimum horizontal stress or the increase in the depth.

Ensemble permeability tensors for the fracture patterns obtained using Approach 1 are shown in Table 5, along with the eigenvalues (λ_{min} and λ_{max}) and the anisotropy ratio (AR) of the permeability tensors defined as $AR = \lambda_{max}/\lambda_{min}$ (Sedaghat et al., 2018). Case 2 shows the lowest permeability with no fractures open (Fig. 3b) whereas in case 3, a large number of fractures are open which create a highly connected horizontal fracture network (Fig. 3c). Deviation from the principal values (eigenvalues) is the lowest for case 2 and the highest for case 3.

Table 6 shows the components of permeability tensor for the fracture patterns obtained using Approach 2. Here, change of aperture due to the increase in σ_h (case 2 vs. case 1 and case 4 vs. case 3) is not as significant as the results from Approach 1. Unlike the results from Approach 1, the increase in depth has resulted in almost even reduction in the aperture sizes for both cases 3 and 4. This is reasonable. A higher value of *AR* indicates a higher value of anisotropy and vice versa. Looking at the last column of Table 6, the anisotropy reduces with depth and with the reduction of difference between the maximum and minimum horizontal stresses.

5. Discussion

Modelling the influence of in situ stresses on the flow properties of fractured rocks is complex in nature. This is mainly due to the complex geometry of fractured rocks and the elaborate mechanical behaviours of such rocks, especially when considering the interaction with flow in fractures. This has encouraged simplifications in modelling. One of the key simplifications is modelling the fractured rock in 2D, ignoring the influence of interaction of the fractured rock layer with other layers and the influence of the overburden stress (e.g. Zhang and Sanderson, 1996; 2002; Min et al., 2004; Latham et al., 2013; Azizmohammadi and Matthai, 2017).

Another simplification is to ignore the influence of the mechanical behaviours of the rock blocks on fracture apertures and to only update the fracture apertures based on the far-field stresses projected on fractures (e.g. Azizmohammadi and Matthai, 2017). This not only ignores the stress variation in the matrix especially when the stress concentrations are around the edges of the fractures and blocks, but also does not consider the interaction between the rock blocks and their displacements and rotations which can directly influence the fracture apertures.

Here, two different approaches are compared. Approach 1 (Azizmohammadi and Matthai, 2017) is a simplified 2D consideration of the change of fracture apertures under the applied stresses, which updates the apertures under the projected far-field stresses. Approach 2 uses a 3D mechanical simulation for calculating the fracture apertures under applied stresses considering the influence of the interaction between rock layers and rock blocks on the fracture apertures. The updated fracture aperture maps from both approaches are used for estimation of permeability tensor by running single-phase flow simulations in two perpendicular directions.

Results from Approaches 1 and 2 were found to be similar for cases 1 and 4. A consistent pattern was observed for the permeability results of Approach 2 in which the permeability reduced with the increase of the minimum horizontal stress, σ_h, for a constant σ_H. Also, with the increase of depth, i.e. higher σ_v, the permeability of the fracture network was reduced as expected for most cases. However, the results of Approach 1 showed an increase in permeability with the increase of depth, with a sudden jump in the permeability of case 3 (15.6 times that of case 1 for the k_{xx} component of the permeability tensor). Results from Approach 1 also suggested an excessive sensitivity to small changes of σ_h with a full closure of fractures in case 2 and 79 times reduction in k_{xx} permeability component of case 4 compared to case 3, due to only 8.3% increase in σ_h. The observed trends in the results of Approach 1 did not seem to be reasonable as also suggested in comparison with the results from Approach 2. These could potentially be related to the unrealistic definition of boundary conditions in Approach 1, i.e. ignoring the influence of σ_v and the neighbouring layers, whereas the direct projection of the stresses on the fracture walls ignored the stress distribution within the rock layer.

Another effect that is ignored in Approach 1 is the rotation, displacement and deformation of rock blocks which, if considered, can increase the fracture apertures and as a result the ensemble permeability. This deficiency can be a reason for the excessive sensitivity of the results of Approach 1 to the increase of σ_h.

Table 5
Components of permeability tensor for the fracture patterns obtained using Approach 1.

Case	Test description		Permeability (10^{-13} m^2)				Eigenvalues (10^{-13} m^2)		$AR = \frac{\lambda_{max}}{\lambda_{min}}$
	Depth (m)	σ_h (MPa)	k_{xx}	k_{xy}	k_{yx}	k_{yy}	λ_{min}	λ_{max}	
1	500	$0.6\sigma_v$	6.37	−2.6	−2.6	1.56	1.55	6.39	4.12
2	500	$0.65\sigma_v$	1	0	0	1	1	1	1
3	1500	$0.6\sigma_v$	99.5	2.14	2.14	7.5	7.45	99.6	13.37
4	1500	$0.65\sigma_v$	1.26	0.028	0.028	1.01	1	1.27	1.27

Table 6
The components of permeability tensor for the fracture patterns obtained using Approach 2.

Case	Test description		Permeability (10^{-13} m^2)				Eigenvalues (10^{-13} m^2)		$AR = \frac{\lambda_{max}}{\lambda_{min}}$
	Depth (m)	σ_h (MPa)	k_{xx}	k_{xy}	k_{yx}	k_{yy}	λ_{min}	λ_{max}	
1	500	$0.6\sigma_v$	6.345	0.217	0.289	2.666	2.64	6.36	2.4
2	500	$0.65\sigma_v$	5.988	0.237	0.351	2.969	2.94	6.01	2.04
3	1500	$0.6\sigma_v$	2.449	−0.044	−0.057	1.715	1.71	2.542	1.48
4	1500	$0.65\sigma_v$	2.17	−0.021	−0.043	1.631	1.629	2.171	1.33

6. Conclusions

This study investigated and compared two different approaches for the calculation of aperture change in fragmented rocks due to the applied in situ stresses. The first approach considers the fragmented rock layer in 2D and ignores the influence of overburden stress and the neighbouring layers. It also projects the horizontal in situ stresses directly to the fracture walls without performing a stress–strain analysis of the entire rock layer. The second approach considers a 3D model of the fragmented rock layer with two softer neighbouring layers above and below the fragmented layer, which allows for a more realistic representation of the boundary stresses. Approach 2 conducts a stress–strain analysis of the entire model including the fragmented rock layer and the neighbouring layers, where the frictional interfaces between the layers and at the interactions between the rock blocks are considered. This allows for the simulation of the rotation, displacement, and deformation of the rock blocks.

Four different scenarios including two different burial depths and two different ratios of σ_h/σ_H were modelled using both approaches (eight models in total). Flow simulations were conducted for all cases with updated fracture apertures in two perpendicular directions to obtain permeability tensors. Results from Approach 2 suggested that permeability was reduced with the increase of σ_h/σ_H ratio and the increase of the burial depth. However, results from Approach 1 showed an increase in the permeability by the increase of depth and an excessive sensitivity to small changes in σ_h/σ_H ratio, which did not seem to be correct.

The simplifications used in Approach 1 reduced the analysis time, however, it caused inaccuracies in the results. Due to the realistic modelling of the mechanical behaviour of the fragmented rock layer in Approach 2, it resulted in more accurate predictions of fracture apertures and the ensemble permeability. Despite the observed inaccuracies in Approach 1, its results can still provide a simple and quick indication of the range of the fracture apertures and ensemble permeability. However, one must be aware of the potential errors that may occur due to the simplified assumptions used in this approach.

Conflicts of interest

The authors wish to confirm that there are no known conflicts of interest associated with this publication and there has been no significant financial support for this work that could have influenced its outcome.

Appendix A. Supplementary data

Supplementary data to this article can be found online at https://doi.org/10.1016/j.jrmge.2018.05.003.

References

Agheshlui H, Matthai S. Uncertainties in the estimation of in situ stresses: effects of heterogeneity and thermal perturbation. Geomechanics and Geophysics for Geo-energy and Geo-resources 2017;3(4):415–38.

Agheshlui H, Sedaghat MH, Matthai S. Stress influence on fracture aperture and permeability of fragmented rocks. Journal of Geophysical Research: Solid Earth 2018;123. https://doi.org/10.1029/2017JB015365.

Azizmohammadi S, Matthai SK. Is the permeability of naturally fractured rocks scale dependent? Water Resources Research 2017;53(9):8041–63.

Bandis SC, Lumsden AC, Barton NR. Fundamental of rock joint deformation. International Journal of Rock Mechanics and Mining Science & Geomechanics Abstracts 1983;20(6):249–68.

Barton N, Choubey V. The shear strength of rock joints in theory and practice. Rock Mechanics 1977;10(1–2):1–54.

Barton N, Bandis S. Effects of block size on the shear behavior of jointed rock. Berkeley, California, USA: American Rock Mechanics Association; 1982.

Barton N, Bandis S, Bakhtar K. Strength, deformation and conductivity coupling of rock joints. International Journal of Rock Mechanics and Mining Sciences & Geomechanics Abstracts 1985;22(3):121–40.

Bazrafkan S, Matthai S. A new hybrid simulation method for multiphase flow on unstructured grids with discrete representations of material interfaces. In: IAMG salzburg 2011, salzburg proceedings. IAMG; 2011. p. 294–305.

Byerlee JD. Friction of rock. Pure and Applied Geophysics 1978;116(4–5):615–26.

Coulomb CA. Sur une application des regles de maximums et minimums a quelques problemes de statistique relatifs a larchitesture. Academy Royal Science Memorial Mechanical Minimal Science 1773;7:343–82 (in French).

Durlofsky LJ. Representation of grid block permeability in coarse scale models of randomly heterogeneous porous media. Water Resources Research 1992;28(7):1791–800.

Kranzz R, Frankel A, Engelder T, Scholz C. The permeability of whole and jointed Barre granite. International Journal of Rock Mechanics and Mining Sciences & Geomechanics Abstracts 1979;16(4):225–34.

Lang P, Steinecker S, Afkan SB, Matthai SK. Stress dependent anisotropy of relative permeabilities in naturally fractured reservoirs. In: ECMOR XIII - 13th european conference on the mathematics of oil recovery. Bairritz, France: EAGE; 2012. https://doi.org/10.3997/2214-4609.20143235.

Latham JP, Xiang J, Belayneh M, Nick HM, Tsang CF, Blunt MJ. Modelling stress-dependent permeability in fractured rock including effects of propagating and bending fractures. International Journal of Rock Mechanics and Mining Sciences 2013;57:100–12.

Lei Q, Wang X, Xiang J, Latham JP. Polyaxial stress-dependent permeability of a three-dimensional fractured rock layer. Hydrogeology Journal 2017;25(8):2251–62.

Malvern LE. Introduction to the mechanics of a continuous medium. Prentice-Hall; 1969.

Matthai SK, Nick HM. Upscaling two-phase flow in naturally fractured reservoirs. AAPG Bulletin 2009;93(11):1621–32.

Matthai S, Bazrafkan S, Lang P, Milliotte C. Numerical prediction of relative permeability in water-wet naturally fractured reservoir rocks. In: ECMOR XIII-13th european conference on the mathematics of oil recovery. EAGE; 2012. https://doi.org/10.3997/2214-4609.20143167.

Matthai S, Bazrafkan S, Mindel J. The finite-element-centered finite-volume discretization method (FECFVM) for multiphase transport in porous media with sharp material discontinuities. In: ECMOR XIV-14th european conference on the mathematics of oil recovery; 2014. https://doi.org/10.3997/2214-4609.20141841.

Min KB, Rutqvist J, Tsang CF, Jing L. Stress-dependent permeability of fractured rock masses: a numerical study. International Journal of Rock Mechanics and Mining Sciences 2004;41(7):1191–210.

Paluszny A, Matthai SK, Hohmeyer M. Hybrid finite element–finite volume discretization of complex geologic structures and a new simulation workflow demonstrated on fractured rocks. Geofluids 2007;7(2):186–208.

Sedaghat MH, Azizmohammadi S, Matthai SK. Numerical investigation of fracture-rock matrix ensemble saturation functions and their dependence on wettability. Journal of Petroleum Science and Engineering 2017;159:869–88.

Sedaghat M, Matthai S, Azizmohammadi S. Tensorial fracture-matrix ensemble relative permeabilities in naturally fractured reservoirs: evidence from discrete fracture and matrix simulations. In: The third EAGE workshop on naturally fractured reservoirs. Muscat, Oman: EAGE; 2018. https://doi.org/10.3997/2214-4609.201800044.

Zhang X, Sanderson DJ. Effects of stress on the two-dimensional permeability tensor of natural fracture networks. Geophysical Journal International 1996;125(3):912–24.

Zhang X, Sanderson DJ, Barker AJ. Numerical study of fluid flow of deforming fractured rocks using dual permeability model. Geophysical Journal International 2002;151(2):452–68.

Zienkiewicz OC. The finite element method. London: McGraw Hill Higher Education; 1977.

Zoback MD. Reservoir geomechanics. Cambridge University Press; 2007.

Dr. Hossein Agheshlui received his BSc degree in Civil Engineering and MSc degree in Marine Structures Engineering from KNT University of Technology, Tehran, Iran. He completed his PhD in Structural Engineering in 2014 from The University of Melbourne, Australia during which he focused on the development of a novel structural connection for use in concrete structures, focusing on studying concrete behaviour under complex stress states involving damaged plasticity constitutive models and concrete cracking and crushing. He has several years of industry experience in oil and gas, infrastructure and building sectors. His interest in continuum mechanics motivated him to investigate more complex problems of subsurface engineering involving fractured rocks including fluid flow through fractures as a research fellow at The University of Melbourne. He also has lectured structural engineering subjects at that university for a few years. His main research areas include continuum mechanics, nonlinear finite element modelling, subsurface geomechanics, and steel-concrete composite structures. He has published several papers in the top of the field journals and has presented in international conferences in these areas.